

# Robust Active Vibration Isolation: A Multivariable Data-Driven Approach

Rick van der Maas\* Tom Oomen\*

\* Eindhoven University of Technology, Control Systems Technology,  
PO Box 513, Building GEM-Z, 5600 MB, Eindhoven, The Netherlands  
R.J.R.v.d.Maas@tue.nl, T.A.E.Oomen@tue.nl

---

**Abstract:** Active vibration isolation is essential for a large range of high precision motion systems in industry. This paper aims to develop a framework for high performance robust vibration isolation by explicitly addressing multivariable flexible dynamical behavior. A framework is proposed that connects identification and control. In addition, a new data-driven uncertainty modeling procedure is used that results in a nonconservative model error bound. Application on an active vibration isolation system confirms high performance robust vibration isolation.

---

## 1. INTRODUCTION

For actively controlled vibration isolation, robustness in the controller design is of key importance. A challenging example is an active vibration isolation system (AVIS), see Fig. 1. These systems are used to isolate high accuracy motion systems from external disturbances in multiple degrees-of-freedom. The idea of active vibration isolation is based on the concept of skyhook damping, see, *e.g.*, Karnopp [1995]. Model-based design procedures based on  $\mathcal{H}_\infty$ -optimization, which are especially suitable for multivariable systems are considered in Zhang et al. [2005] and Chida et al. [2008]. In Zhang et al. [2005] model uncertainty is explicitly taken into account. However, the uncertainty is based on rough prior assumptions, leading to potential conservative results.

Several identification methodologies have been developed to obtain good models that are suitable for such  $\mathcal{H}_\infty$  control algorithms. In Schrama [1992], identification for control using coprime factorizations is proposed. This work is further extended to model sets by de Callafon and Van den Hof [1997], enabling the identification of a robust-control-relevant model. By introducing specific coprime factorizations of the plant and the controller, an additional degree of freedom is obtained to shape the uncertainty structure. In Oomen and Bosgra [2012], the additional degree of freedom of the coprime factorizations is exploited, enabling a direct connection between the  $\mathcal{H}_\infty$ -norm bounded size of the model uncertainty and the performance criterium for robust control.

Besides the nominal model, the estimation of the size of model uncertainty is critical for  $\mathcal{H}_\infty$  robust control design. To estimate this uncertainty size, model-error modeling techniques have been developed based on existing system identification techniques, see Reinelt et al. [2002], or based on nonparametric approaches by van de Wal et al. [2002] and de Vries and Van den Hof [1994]. The main drawback of these methods are the resulting intergrid errors, which is unavoidable using finite time experiments. Bounding these intergrid errors, generally result in overly large uncertainty estimates, as is also argued in Vinnicombe [2001, Sec. 9.5.2]. In addition, many model validation techniques have been proposed, see Smith and Doyle [1992] for a time domain approach and Poolla et al. [1994] for a frequency domain approach. Proper experiment design is key to

obtain accurate uncertainty estimations. Iterative data-driven procedures for  $\mathcal{H}_\infty$ -estimations are proposed by Hjalmarsson [2005, Sec. 12.2] and Wahlberg et al. [2010] followed by a thorough stochastic analysis in Rojas et al. [2012]. An application in robust stability analysis of the procedures can be found Barenthin et al. [2006]. An extension for multivariable systems is given in Oomen et al. [2014].

Although important developments have been made in identification for robust control, at present these techniques have not been exploited for high performance robust active vibration isolation. The main contribution of this paper is the use of the data-driven approach as introduced in Oomen et al. [2014] in a framework that directly connects identification and control to improve the performance for an active vibration isolation system. To enhance the performance, it is key to choose a specific model uncertainty structure as proposed in Oomen and Bosgra [2012]. As a result, enhanced robust control of an industrial vibration isolation system is obtained. In Sec. 2, the industrial AVIS is introduced and the control goal is defined. In Sec. 3, modeling and identification of the uncertain model set for robust control is presented, followed by the controller synthesis in Sec. 4. Finally, the work is concluded in Sec. 5.

## 2. SYSTEM DESCRIPTION AND CONTROL GOAL

### 2.1 Active Vibration Isolation System

The AVIS in Fig. 1 is considered in this paper. The system consists of two main parts, a chassis connected to the floor and a movable top or payload. These two parts are connected by four isolator modules that provide passive damping through a pneumatic airmount. In addition to the passive damping, the modules are equipped with Lorentz actuators and geophones that enable active vibration isolation. Specifically, the isolation modules are each equipped with two actuators, leading to eight actuators in total. The controlled currents applied to the actuators are denoted  $a = [a_1 \ a_2 \ a_3 \ a_4 \ a_5 \ a_6 \ a_7 \ a_8]$ . In addition, three out of four modules are equipped with two geophones each, leading to a total of six sensors, denoted by,  $s = [s_1 \ s_2 \ s_3 \ s_4 \ s_5 \ s_6]$ . The inputs and outputs of the system are rigid-body decoupled with respect to the



Fig. 1. Photograph of the experimental AVIS setup. The rotation around the  $x$ -axis is denoted by  $\phi$ .

cartesian coordinate frame depicted in Fig. 1. The actual manipulated input and output signals are denoted by,

$$u = T_u a \quad (1)$$

$$y = T_y s, \quad (2)$$

respectively, where  $T_u \in \mathbb{R}^{6 \times 8}$  and  $T_y \in \mathbb{R}^{6 \times 6}$ . The true system  $P_o$  is given by,  $P_o : u \mapsto y$ .

The main goal of an AVIS is isolation of the payload with respect to exogenous disturbances. The considered AVIS in this work is schematically illustrated in Fig. 2. The signal  $d_1$  refers to force disturbances directly acting on the payload, and  $d_2$  refers to force disturbances that are induced by floor vibrations. The goal is to minimize the absolute velocity of the payload using the actively controlled input  $u$  through the absolute velocity measurement  $y$ , enabling skyhook damping (Karnopp [1995]). Skyhook damping connects a fictive damper (implemented as a control algorithm) to the fixed world, which directly implies that  $y$  in Fig. 2 should be minimized in the presence of the disturbances  $d_1$  and  $d_2$ . This is in sharp contrast to the situation where only measurements relative to the floor are available, in which case  $y$  should be minimized only in the case  $d_2 = 0$ . The resulting feedback interconnection is shown in Fig. 3, where,

$$d = d_1 + H_d d_2, \quad (3)$$

with  $H_d$  a causal stable transfer function matrix that characterizes the transfer of the floor vibrations through the pneumatic airmount to the payload.

To show the potential performance improvement by skyhook damping, an initial controller  $C^{\text{exp}}$  is designed. This controller consists of a multi-loop SISO controller, where each diagonal element is a gain with high-frequency roll-off, see Fig. 8 for the diagonal elements corresponding to the  $z$  and  $\phi$  directions. The resulting closed-loop transfer function

$$P_o^{\text{cl,exp}} : d \mapsto y = P_o(I + C^{\text{exp}} P_o) \quad (4)$$

characterizes the closed-loop disturbance attenuation properties. In Fig. 9 in Section 4.1, frequency response function measurements of the open-loop system  $P_o$  and the closed-loop system  $P_o^{\text{cl,exp}}$  are depicted.

## 2.2 Control Goal and Approach

The objective of this paper is the design of a high performance robust controller to improve vibration isolation properties of an AVIS. The key performance limiting factor in increasing the gain of an initial experimental controller  $C^{\text{exp}}$ , which is similar to increasing the skyhook damping, are high-frequency flexible dynamics of the system as can be observed in Fig. 9. In this paper, a model-based

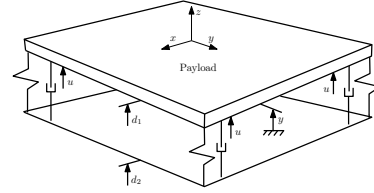


Fig. 2. Schematic illustration of the AVIS.

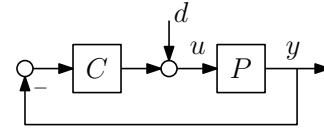


Fig. 3. Simplified feedback interconnection for vibration isolation.

controller design is pursued that requires appropriately specified performance and robustness objectives. The performance objectives are specified using a criterion  $\mathcal{J}(P, C)$ , where the goal is to compute the optimal controller that minimizes  $\mathcal{J}(P_o, C)$ , requiring accurate knowledge of  $P_o$ . Due to the fact that any model is uncertain and is only an approximation of the true system behavior, a model set  $\mathcal{P}$  is defined. The key property of this model set  $\mathcal{P}$  is that it is chosen such that it includes all AVIS dynamical behavior, *i.e.*, including high-frequency flexible dynamics. Hence,

$$P_o \in \mathcal{P} \quad (5)$$

always holds. Using (5), given the model set  $\mathcal{P}$ , the robust controller synthesis

$$C^{\text{RP}} = \arg \min_C \mathcal{J}_{WC}(\mathcal{P}, C), \quad (6)$$

is considered, where  $\mathcal{J}_{WC}(\mathcal{P}, C) = \sup_{P \in \mathcal{P}} \mathcal{J}(P, C)$ . This result provides a performance guarantee when implementing  $C^{\text{RP}}$  on the true system, given (5), the bound

$$\mathcal{J}(P_o, C^{\text{RP}}) \leq \mathcal{J}_{WC}(\mathcal{P}, C^{\text{RP}}) \quad (7)$$

holds. To facilitate the exposition, a two-input two-output robust feedback controller is designed for the  $z$  and  $\phi$  direction, *i.e.*,

$$\begin{bmatrix} u_z \\ u_\phi \end{bmatrix} = C^{\text{RP}} \begin{bmatrix} y_z \\ y_\phi \end{bmatrix}. \quad (8)$$

The presented approach applies equally well to the full multivariable situation, *i.e.*, three rotations and three translations. In this paper, the selection of a rotational and translational degree-of-freedom is made to show that the presented approach automatically deals with the various units of the measurements.

## 2.3 Control Criterion

The control goal in this paper is specified by,

$$\mathcal{J} = \|WT(P, C)V\|_\infty, \quad (9)$$

where,

$$T(P, C) = \begin{bmatrix} T_{11} & T_{12} \\ T_{21} & T_{22} \end{bmatrix} = \begin{bmatrix} P \\ I \end{bmatrix} (I + CP)^{-1} [C \ I]. \quad (10)$$

and

$$T(P, C) : \begin{bmatrix} r_2 \\ r_1 \end{bmatrix} \mapsto \begin{bmatrix} y \\ u \end{bmatrix}. \quad (11)$$

Here  $r_1$  corresponds to  $d$  in Fig. 3 and  $r_2$  is an additional signal, see Fig. 6 for a block diagram. In addition,  $W$  and  $V$  in (9) are stable, minimum-phase weighting filters.

The four-block problem in (10) guarantees internal stability of the resulting optimal controller. This has important implications from a theoretical perspective, since it will enable the construction of a specific coprime factorization that leads to (20). In addition, the four-block problem enables the use of the systematic loop-shaping approach in McFarlane and Glover [1990] to select  $W$  and  $V$  such that it enhances active vibration isolation performance. Interestingly, the loop-shaping approach in McFarlane and Glover [1990] is essentially based on the fact that the loop-gain  $CP$  is the only degree of freedom in (10). In Fig. 11 it is shown that for low frequencies the system reduces the disturbances  $d_1$  and  $d_2$ .

In the considered design framework, so-called loop-shaping weighting filters  $W_1$  and  $W_2$  are adopted that shape the desired open-loop gain  $W_2PW_1$ . Next, observe that the initial controller leads to a certain loop-gain  $C^{\text{exp}}P$ . The desired loop-gain typically has a smaller amplitude in the low frequency range compared to  $W_2PW_1$ . Hence, the rationale in this paper to design the weighting filter  $W_1$  and  $W_2$  is to increase the gain of  $C^{\text{exp}}$ , *i.e.*,

$$W_1 = \begin{bmatrix} 1 & 0 \\ 0 & 1 \end{bmatrix}, \quad W_2 = \begin{bmatrix} 19.9 & 0 \\ 0 & 11.75 \end{bmatrix} C^{\text{exp}}. \quad (12)$$

Although the design procedure to select  $W_2$  resembles the controller  $C^{\text{exp}}$ , a robust controller synthesis procedure is required to deliver a robustly stabilizing feedback controller. These weighting functions  $W_2$  and  $W_1$  directly fit in criterion (9) through  $W = \begin{bmatrix} W_2 & 0 \\ 0 & W_1^{-1} \end{bmatrix}, V = \begin{bmatrix} W_2^{-1} & 0 \\ 0 & W_1 \end{bmatrix}$ .

#### 2.4 Obtaining $\mathcal{P}$ using $\mathcal{H}_\infty$ -norm bounded Perturbations

The uncertain model set  $\mathcal{P}$  that is introduced in Sec. 2.2 is constructed as an  $\mathcal{H}_\infty$  norm bounded perturbation around a nominal model  $\hat{P}$ , *i.e.*,

$$\mathcal{P} = \left\{ P \mid P = \mathcal{F}_u(\hat{H}(\hat{P}), \Delta_u), \Delta_u \in \mathbf{\Delta}_u \right\}, \quad (13)$$

where  $\hat{H}(\hat{P})$  represents the nominal model  $\hat{P}$  and uncertainty structure. Also, the upper linear fractional transformation (LFT) is given by

$$\mathcal{F}_u(\hat{H}, \Delta_u) = \hat{H}_{22} + \hat{H}_{21}\Delta_u(I - \hat{H}_{11}\Delta_u)^{-1}\hat{H}_{12}. \quad (14)$$

In addition, to anticipate on the results in Sec. 3.3, an unstructured model uncertainty is considered, *i.e.*,

$$\mathbf{\Delta}_u := \{ \Delta_u \mid \|\Delta_u\|_\infty \leq \gamma \} \quad (15)$$

To actually identify  $\mathcal{P}$ , the required three step procedure is summarized as follows.

*Procedure 1.* Perform the following three steps for identification of  $\mathcal{P}$ :

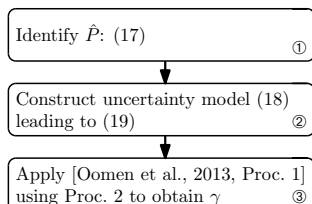


Fig. 4. Three step procedure for identification of (13)

In this paper, the novel iterative data-driven approach for multivariable systems as presented in Oomen et al. [2014] is used to obtain the size of the uncertainty  $\gamma$  purely data-based. Emphasis is on the application of the procedure for

uncertainty modelling for vibration isolation applications, while the complete procedure that encompasses steps 1)-3) of Proc. 1 is addressed.

### 3. MULTIVARIABLE MODELING PROCEDURE FOR ACHIEVING ROBUST PERFORMANCE

As is argued in Sec. 2.4, two aspects determine the shape of the model set  $\mathcal{P}$ , *i.e.*, 1) the nominal model  $\hat{P}$ , and 2) the uncertainty structure leading to  $\hat{H}(\hat{P})$  in (13).

The size and shape of the model set  $\mathcal{P}$  contribute to the worst-case performance bound in (7). In this section, the three steps of Proc. 1 are used to jointly obtain a nominal model  $\hat{P}$ , the uncertainty structure,  $\hat{H}(\hat{P})$ , and an estimation of  $\gamma$  that aims at achieving a small worst-case performance bound in (7).

First, the general objective for modeling  $\mathcal{P}$  is defined in Sec. 3.1, after which the three steps are described in detail in Sec. 3.2-3.4.

#### 3.1 Modeling goal

The function  $\mathcal{J}_{WC}(\mathcal{P}, C)$  is a complex function of both  $\mathcal{P}$  and  $C$ . By noting that  $C^{\text{RP}}$  in (6) depends on  $\mathcal{P}$ , *i.e.*,  $C^{\text{RP}}(\mathcal{P})$ , it is desired to determine  $\mathcal{P}$  such that it minimizes  $\mathcal{J}_{WC}(\mathcal{P}, C^{\text{RP}}(\mathcal{P}))$ , subject to (5). However, this is in general difficult to solve.

The key step in this section is to exploit knowledge of  $C^{\text{exp}}$ , see Sec. 2.1, to obtain a tractable approach that is aimed at achieving high performance in (6). Note that  $\mathcal{J}_{WC}(\mathcal{P}, C^{\text{RP}}) \leq \mathcal{J}_{WC}(\mathcal{P}, C^{\text{exp}})$ . Hence  $C^{\text{exp}}$  provides an upper bound for the guaranteed performance in (6). Hence, as in Oomen and Bosgra [2012] and de Callafon and Van den Hof [1997], the aim is to determine

$$P = \arg \min \mathcal{J}_{WC}(P, C^{\text{exp}}) \quad \text{subject to } P_o \in \mathcal{P}. \quad (16)$$

#### 3.2 Step I: nominal modeling

In the first step of Proc. 1, a nominal model  $\hat{P}$  is identified. In particular, the control-relevant identification criterion in Schrama [1992] is adopted, *i.e.*,  $\hat{P}$  is minimized according to

$$\min_{\hat{P}} \left\| WT(P_o, C^{\text{exp}})V - WT(\hat{P}, C^{\text{exp}})V \right\|_\infty. \quad (17)$$

The actual minimization in (17) is performed using the approach in Oomen and Bosgra [2012]. It is shown in Sec. 3.3 that this criterion is useful in view of (16).

The first step in obtaining the nominal model  $\hat{P}$  in (17), is the measurement of a frequency response function of the closed-loop system  $T(P_o, C^{\text{exp}})$  using the approach in Pintelon and Schoukens [2012]. The main reason for the intermediate step of frequency response function identification is that it enables the solution of (17) by exploiting the frequency domain interpretation of the  $\mathcal{H}_\infty$ -norm. By exploiting a multisine experiment design, the approach in Pintelon and Schoukens [2012] enables accurate identification of frequency response functions by effectively reducing the variance error without introducing bias. By virtue of (10), an estimate of  $P$  can be obtained from the relation  $P = T_{12}T_{22}^{-1}$ . The identified frequency response function of  $P_o$  is depicted in Fig. 5. Next, a model parametrization for  $\hat{P}$  is obtained by an 8<sup>th</sup> order model. The reason for

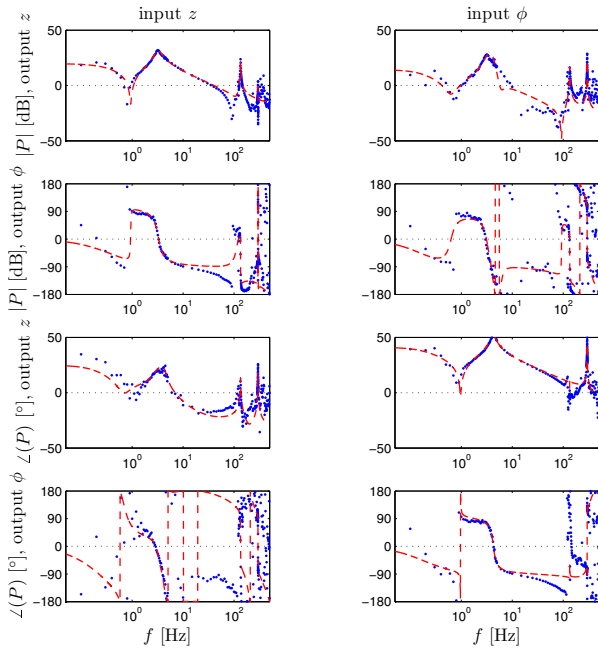


Fig. 5. Nonparametric frequency response function  $P_o$  (blue dots) and identified parametric model  $\hat{P}$  (dashed red). Both the  $z$ -translation and  $\phi$ -rotation are displayed.

this low order is that the criterion (17) essentially shapes the bias of the parametric model. The actual optimization is performed using the algorithm in Oomen and Bosgra [2012, Sec. 3.4-3.5]. The resulting parametric model  $\hat{P}$  is also depicted in Fig. 5. Inspection reveals that the suspended rigid-body mode at 4 [Hz] and the first resonance at 135 [Hz] are accurately modeled.

### 3.3 Step II: uncertainty model structure selection

In this step, the main contribution of this work is introduced, which enables a direct connection between the size  $\gamma$  of the uncertainty discussed in step III in Sec. 3.4, and the performance criterion. Having identified a nominal model that minimizes (17), the next step is the selection of an uncertainty model structure that extends  $\hat{P}$  to  $\hat{H}(\hat{P})$ . As in Step I, the essence lies in selecting the uncertainty structure such that it facilitates solving (17).

To establish the connection between  $\hat{H}(\hat{P})$  and the criterion (16), note that the latter can be expressed as an LFT. This involves the construction of a generalized plant as is explained in Skogestad and Postlethwaite [2005, Sec. 3.8]. In particular, the uncertainty model  $\mathcal{P}$  in (13) is appended with weighting filters and interconnected with  $C^{\text{exp}}$ , leading to the setup in Fig. 6. As a result,

$$\mathcal{J}_{WC}(\mathcal{P}, C^{\text{exp}}) = \sup_{\Delta_u \in \Delta_u} \left\| \hat{M}_{22} + \hat{M}_{21} \Delta_u (I - \hat{M}_{11} \Delta_u)^{-1} \hat{M}_{12} \right\|_{\infty}. \quad (18)$$

Since (18) depends in a complicated manner on  $\Delta_u$  and hence  $\gamma$ , see (15), a specific approach that relies on the results in Oomen and Bosgra [2012] is adopted. In particular in Oomen and Bosgra [2012], it is suggested to

- i. adopt the dual-Youla uncertainty structure Douma and Van den Hof [2005], de Callafon and Van den Hof [1997]

$$\mathcal{P}^{\text{DY}} = \left\{ P \mid P = (\hat{N} + D_c \Delta_u)(\hat{D} - N_c \Delta_u)^{-1}, \Delta_u \in \Delta_u \right\}, \quad (19)$$

where,

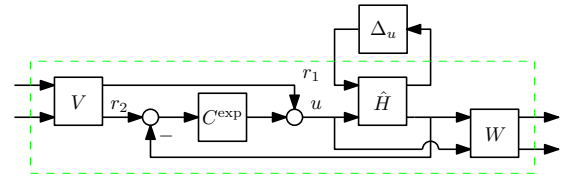


Fig. 6. Worst-case performance  $\mathcal{J}_{WC}(\mathcal{P}, C)$  cast into the generalized plant framework.

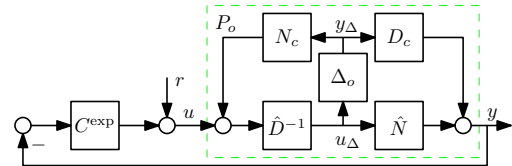


Fig. 7. Block diagram corresponding to uncertainty structure 19.

- ii. the pair  $\{\hat{N}, \hat{D}\}$  is a robust-control-relevant coprime factorization of  $\hat{P}$  as defined in Oomen and Bosgra [2012, Sec. 3.3], and
- iii. the pair  $\{N_c, D_c\}$  as a  $(W_u, W_y)$ -normalized coprime factorization of  $C^{\text{exp}}$ , see Oomen and Bosgra [2012].

As a result of i - iii, (18) simplifies to

$$\mathcal{J}_{WC}(\mathcal{P}, C^{\text{exp}}) \leq \|\hat{M}_{22}\|_{\infty} + \sup_{\Delta_u \in \Delta_u} \|\Delta_u\|_{\infty} = \mathcal{J}(\hat{P}, C^{\text{exp}}) + \gamma, \quad (20)$$

see Oomen and Bosgra [2012] for a proof of (20) and more details of the specific coprime factorizations.

The result of (20) provides a direct connection between the size  $\gamma$  of  $\Delta_u$ , see (15), and the control criterion  $\mathcal{J}_{WC}(\mathcal{P}, C^{\text{exp}})$ . Interestingly, the size of the model uncertainty  $\gamma$  in (20) is equal to the norm in the control-relevant identification objective (17). This implies that the same objective is being pursued during the nominal model step in Sec. 3.2 and during the uncertainty modeling step discussed in the current section. In the upcoming section, the final step leading to the size  $\gamma$  is presented, enabling the construction of  $\mathcal{P}$  in (13).

### 3.4 Step III: data-driven estimation of $\gamma$

Now, given  $\hat{H}(\hat{P})$ , it remains to estimate  $\gamma$  to complete the model set  $\mathcal{P}$ . In this step,  $\gamma$  is estimated using the multivariable data-driven  $\mathcal{H}_{\infty}$ -norm estimation procedure as described in detail in Oomen et al. [2014, Proc. 2].

The key advantage is that direct measurements are performed on  $\Delta_o$  and thus no explicit a priori knowledge is required to obtain  $\|\Delta_o\| = \gamma$ . As is illustrated in Oomen et al. [2014], the procedure can be applied to any open-loop identification problem. The first step in this section is to investigate how to gain access to the signals  $u_{\Delta}$  and  $y_{\Delta}$ , given the uncertainty structure in (19). Note that the  $\Delta_o$  corresponding to  $P_o$  can be computed directly using (19), leading to

$$\Delta_o = D_c^{-1}(I + P_o C)^{-1}(P_o - \hat{P})\hat{D}. \quad (21)$$

The result in (21) reveals that  $\Delta_o$  depends on the model  $\hat{P} = \hat{N}\hat{D}^{-1}$ , the true system  $P_o$ , and  $C^{\text{exp}} = N_c D_c^{-1}$ .

To gain access to  $u_{\Delta}$  and  $y_{\Delta}$ , note that (19) in closed-loop with  $C^{\text{exp}}$  implemented can be represented as in Fig. 7. Inspection reveals that

$$u_{\Delta} = \hat{D}^{-1}(r - C^{\text{exp}} \hat{N} u_{\Delta} - C^{\text{exp}} D_c y_{\Delta} + N_c y_{\Delta}), \quad (22)$$

implying that the reference signal

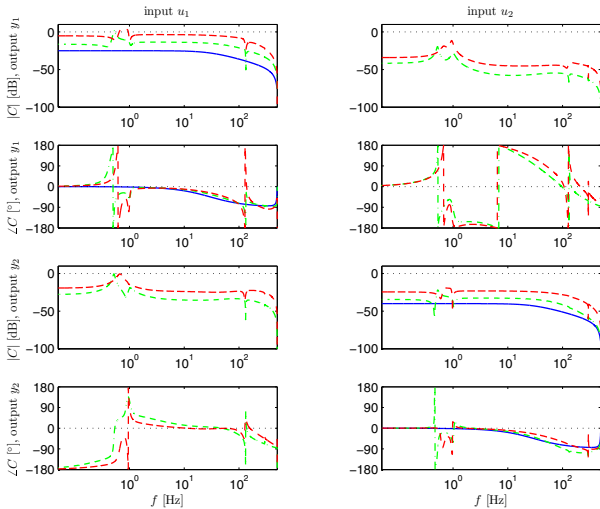


Fig. 8. Controllers:  $C^{\text{exp}}$  (solid blue),  $C^{\text{NP}}$  (dashed red),  $C^{\text{RP}}$  (dashed-dotted green).

$$r = (\hat{D} + C^{\text{exp}} \hat{N}) u_{\Delta} \quad (23)$$

should be applied. Next observe that

$$y_{\Delta} = D_c^{-1} (y - \hat{P}(I + C^{\text{exp}} \hat{P})^{-1} r). \quad (24)$$

The result in (23) and (24) reveals how experiments can directly be performed on  $\Delta_o$  as summarized in the following procedure.

*Procedure 2.* (Performing experiments on  $\Delta_o$ ): Let input  $u_{\Delta}$  be given and perform the following sequence of steps.

- i. compute  $r = (\hat{D} + C^{\text{exp}} \hat{N}) u_{\Delta}$ .
- ii. Perform a closed-loop experiment on  $P_o$  with  $C^{\text{exp}}$  implement, *i.e.*,  $y = P_o(I + C^{\text{exp}} P_o)^{-1} r$ .
- iii. Compute  $y_{\Delta} = D_c^{-1} (y - \hat{P}(I + C^{\text{exp}} \hat{P})^{-1} r)$ .

Proc. 2 can directly be implemented in Oomen et al. [2014, Proc. 2]. enabling the data-driven estimation for multivariable uncertainty structures given by (19).

The resulting  $\mathcal{H}_{\infty}$ -norm estimation of the multivariable  $\Delta_o$  of the AVIS using the data-driven approach is given by  $\hat{\gamma}_2^{(40)} = 1.997$ . See Oomen et al. [2014] for a detailed description and analysis of the iterative data-driven procedure.

## 4. CONTROLLER SYNTHESIS AND EXPERIMENTAL IMPLEMENTATION

### 4.1 Robust controller synthesis

The model set  $\mathcal{P}$  is used to analyze and synthesize several controllers. These synthesized controller are,

- 1)  $C^{\text{exp}}$ : initial controller that is described in Sec. 2.1.
- 2)  $C^{\text{NP}}$ : nominal controller  $C^{\text{NP}} = \arg \min_C \mathcal{J}(\hat{P}, C)$
- 3)  $C^{\text{RP}}$ : robust controller for model set  $\mathcal{P}$  in (6).

The controllers  $C^{\text{NP}}$  and  $C^{\text{RP}}$  are computed using  $\mathcal{H}_{\infty}$ -optimization and skewed- $\mu$ -synthesis, see Skogestad and Postlethwaite [2005] for details.

The designed controllers are depicted in Fig. 8, whereas the closed-loop process sensitivity functions  $\hat{P}(I + C\hat{P})^{-1}$  are depicted in Fig. 9. In addition, the achieved performance for both the model  $\hat{P}$  and the model set  $\mathcal{P}$  in terms of the

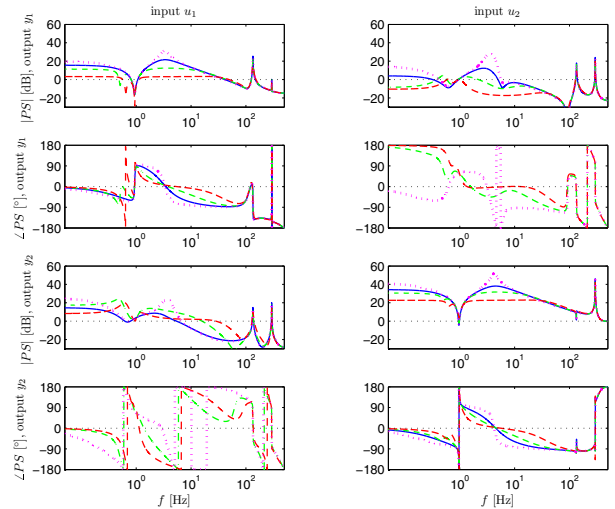


Fig. 9. Closed-loop process sensitivities:  $\hat{P}(I + C^{\text{exp}} \hat{P})^{-1}$  (solid blue),  $\hat{P}(I + C^{\text{NP}} \hat{P})^{-1}$  (dashed red),  $\hat{P}(I + C^{\text{RP}} \hat{P})^{-1}$  (dashed-dotted green). In addition, the nominal model  $\hat{P}$  is depicted (dotted magenta).

Table 1. Robust-control-relevant identification and robust controller synthesis results.

Controller	Minimized criterion	$\mathcal{J}(\hat{P}, C)$	$\mathcal{J}_{WC}(\mathcal{P}, C)$
$C^{\text{exp}}$	None	14.30	16.30
$C^{\text{NP}}$	$\mathcal{J}(\hat{P}, C)$	1.87	$\infty$
$C^{\text{RP}}$	$\mathcal{J}_{WC}(\mathcal{P}, C)$	4.80	5.02

control criterion are presented in Table 1.

The following four observations are made.

- 1) When comparing  $\mathcal{J}(\hat{P}, C^{\text{exp}})$  and  $\mathcal{J}_{WC}(\mathcal{P}, C^{\text{exp}})$ , it is observed that the bound (20) indeed holds and is tight.
- 2) From Table 1,  $C^{\text{NP}}$  indeed achieves optimal performance for the nominal model  $\hat{P}$ . However,  $\mathcal{J}_{WC}(\mathcal{P}, C^{\text{NP}})$  is unbounded.
- 3) The controller  $C^{\text{RP}}$  achieves the smallest worst-case performance, *i.e.*,  $\mathcal{J}_{WC}(\hat{P}, C^{\text{RP}})$  is also significantly improved when compared to  $\mathcal{J}(\hat{P}, C^{\text{exp}})$ .
- 4) In Fig. 8, the resulting controllers are shown, with the nominal controller having a larger gain than the robust controller. In addition, both the nominal and the robust controller are full multivariable controllers, where the initial controller is diagonal.

### 4.2 Controller implementation

The synthesized controllers in Sec. 4.1 are now implemented for validation. Measured time domain responses are depicted in Fig. 10, whereas the corresponding cumulative power spectral densities are depicted in Fig. 11.

The following two observations are made.

- 1) The controller  $C^{\text{NP}}$  does not stabilize the system. This is observed from the response in the  $\phi$ -direction in Fig. 10, where the system hits a safety guardrail due to the unstable behavior. This is in agreement with the results in Table 1, where  $\mathcal{J}_{WC}(\mathcal{P}, C^{\text{NP}})$  is unbounded, and no performance and stability guarantees can be given when implementing  $C^{\text{NP}}$  on the true system  $P_o$ .
- 2) The experimental controller  $C^{\text{exp}}$  and optimal robust controller  $C^{\text{RP}}$  both stabilize the true system, which

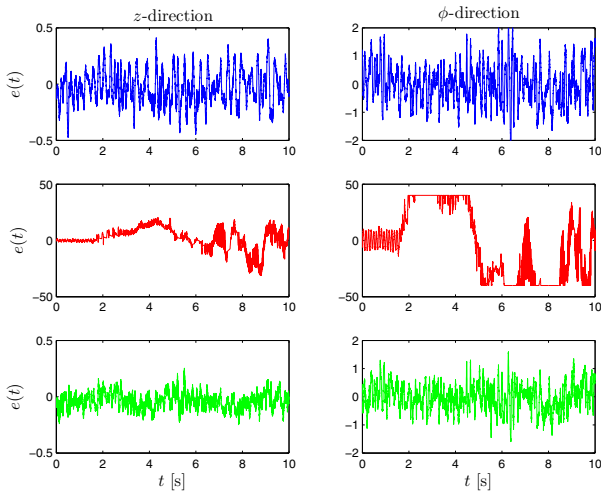


Fig. 10. Measured time domain responses:  $C^{\text{exp}}$  (solid blue, top),  $C^{\text{NP}}$  (dashed red, middle),  $C^{\text{RP}}$  (dashed-dotted green, bottom)

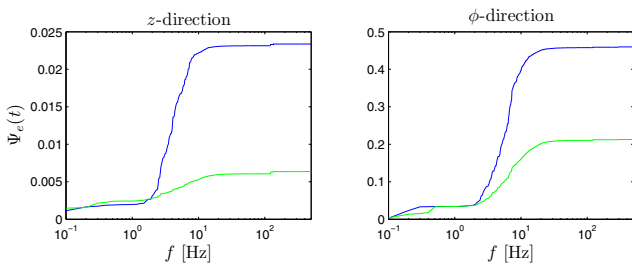


Fig. 11. Cumulative power spectral density (CPS) of the measured error signals in Fig. 10:  $C^{\text{exp}}$  (solid blue, top),  $C^{\text{RP}}$  (dashed-dotted green, bottom).

is revealed by the stationary behavior in Fig. 10. In addition, the controller  $C^{\text{RP}}$  leads to a significantly improved performance when compared to  $C^{\text{exp}}$ , which is visible both from the time domain responses in Fig. 10 as the cumulative power spectra in Fig. 11. In particular, the controller  $C^{\text{RP}}$  leads to a performance improvement of more than a factor 4 in  $z$ -translation and more than a factor 2 in  $\phi$ -rotation.

## 5. DISCUSSION AND CONCLUSION

In this paper, a new framework is proposed for high performance robust active vibration isolation. Using the coprime factorization the problem of identifying  $\Delta_o$  is recast to an open-loop identification problem, enabling the data-driven  $\mathcal{H}_\infty$ -norm estimation leading to the size  $\gamma$ . As a result, an uncertainty bound is obtained that leads to the construction of the model set without introducing additional conservatism with respect to the performance criterion. A three step procedure is provided that enables the construction of the model set, leading to a robust controller that enables enhanced vibration isolation of an industrial AVIS.

## ACKNOWLEDGEMENTS

The authors would like to thank Håkan Hjalmarsson, Christian Rojas, Robbert van Herpen, and Bo Wahlberg for their contribution to this work. In addition, the authors gratefully acknowledge the late Prof. Okko Bosgra for his contributions to this work. This work is supported by the Innovational Research Incentives Scheme

under the VENI grant “Precision Motion: Beyond the Nanometer” (no. 13073) awarded by NWO (The Netherlands Organisation for Scientific Research) and STW (Dutch Science Foundation).

## REFERENCES

- Mårta Barenthin, Martin Enqvist, Bo Wahlberg, and Håkan Hjalmarsson. Gain estimation for Hammerstein systems. In *14th IFAC Symposium on System Identification*, pages 784 – 789, Newcastle, Australia, 2006.
- Yuichi Chida, Yoshiyuki Ishihara, Takuya Okina, Tomoaki Nishimura, Koichi Ohtomi, and Ryo Furukawa. Identification and frequency shaping control of a vibration isolation system. *Control Engineering Practice*, 16(6):711–723, June 2008.
- R. A. de Callafon and P. M. J. Van den Hof. Suboptimal Feedback Control by a Scheme of Iterative Identification and Control Design. *Mathematical Modelling Of Systems*, 3(1):77–101, January 1997.
- Douwe K. de Vries and Paul M. J. Van den Hof. Quantification of model uncertainty from data: input design, interpolation, and connection with robust control design specifications. *International Journal of Robust and Nonlinear Control*, 4(2):301 – 319, 1994.
- Sippe G. Douma and Paul M. J. Van den Hof. Relations between uncertainty structures in identification for robust control. *Automatica*, 41(3):439–457, 2005.
- Håkan Hjalmarsson. From experiment design to closed-loop control. *Automatica*, 41(3):393–438, 2005.
- D. Karnopp. Active and Semi-Active Vibration Isolation. *Transactions of the ASME*, 117(June):177 – 185, 1995.
- D. C. McFarlane and K. Glover. *Lecture Notes in Control and Information Sciences: Robust Controller Design Using Normalized Coprime Factor Plant Descriptions*. Springer-Verlag, 1990.
- Tom Oomen and Okko Bosgra. System identification for achieving robust performance. *Automatica*, 48(9):1975–1987, September 2012.
- Tom Oomen, Rick van der Maas, Cristian R. Rojas, and Hakan Hjalmarsson. Iterative Data-Driven H Norm Estimation of Multivariable Systems With Application to Robust Active Vibration Isolation. *IEEE Transactions on Control Systems Technology*, 2014. doi: 10.1109/TCST.2014.2303047.
- Rik Pintelon and Johan Schoukens. *System Identification: A Frequency Domain Approach*. IEEE Press, New York, NY, USA, 2nd edition, 2012.
- Kameshwar Poolla, Pramod Khargonekar, Ashok Tikku, James Krause, and Krishan Nagpal. A time-domain approach to model validation. *IEEE Transactions on Automatic Control*, 39(5):951–959, May 1994.
- Wolfgang Reinelt, Andrea Garulli, and Lennart Ljung. Comparing different approaches to model error modeling in robust identification. *Automatica*, 38:787–803, 2002.
- Cristian R. Rojas, Tom Oomen, Håkan Hjalmarsson, and Bo Wahlberg. Analyzing iterations in identification with application to nonparametric  $\mathcal{H}_\infty$ -norm estimation. *Automatica*, 48(11):2776–2790, November 2012.
- Ruud J.P. Schrama. Accurate Identification for Control: The Necessity of an Iterative Scheme. *IEEE Transactions on Automatic Control*, 37(7):991 – 994, 1992.
- Sigurd Skogestad and Ian Postlethwaite. *Multivariable Feedback Control, Analysis and Design*. John Wiley & Sons, Inc., 2005.
- Roy S. Smith and John C. Doyle. Model Validation: A Connection Between Robust Control and Identification. *IEEE Transactions on Automatic Control*, 37(7):942–952, 1992.
- Marc van de Wal, Gregor van Baars, Frank Sperling, and Okko Bosgra. Multivariable  $\mathcal{H}_\infty/\mu$  feedback control design for high-precision wafer stage motion. *Control Engineering Practice*, 10: 739–755, 2002.
- Glenn Vinnicombe. *Uncertainty and Feedback:  $\mathcal{H}_\infty$  loop-shaping and the  $v$ -gap metric*. Imperial College Press, London, UK, 2001.
- Bo Wahlberg, Mårta Barenthin Syberg, and Håkan Hjalmarsson. Non-parametric methods for  $\mathcal{L}_2$ -gain estimation using iterative experiments. *Automatica*, 46(8):1376–1381, August 2010.
- Y. Zhang, A.G. Alleyne, and D. Zheng. A hybrid control strategy for active vibration isolation with electrohydraulic actuators. *Control Engineering Practice*, 13(3):279–289, March 2005.